Deubiquitinase UCHL1 Maintains Protein Homeostasis through PSMA7-APEH-Proteasome Axis in High-Grade Serous Ovarian Carcinoma

Apoorva Tangri[1*], Kinzie Lighty[1*], Jagadish Loganathan[1], Fahmi Mesmar[2], Ram Podicheti[3], Chi Zhang[1], Marcin Iwanicki[4], Harikrishna Nakshatri[1,5], Sumegha Mitra[1,5,#]

[1] Indiana University School of Medicine, Indianapolis, IN, USA

[2] Indiana University, Bloomington, IN, USA

[3]Center for Genomics and Bioinformatics, Indiana University, Bloomington, IN, USA

[4]Stevens Institute of Technology, Hoboken, NJ, USA

[5]Indiana University Melvin & Bren Simon Cancer Center, Indianapolis, USA

*Equal contribution

corresponding author; to whom correspondence may be addressed.

E-mail: mitras@indiana.edu

Abstract

High-grade serous ovarian cancer (HGSOC) is characterized by genomic instability, DNA damage, oxidative stress, and high metabolic demand that contribute to misfolded proteins and proteotoxicity. However, the underlying mechanisms that maintain protein homeostasis to promote HGSOC growth remain poorly understood. In this study, we report that the neuronal deubiquitinating enzyme, UCHL1 (ubiquitin C-terminal hydrolase L1) is overexpressed in HGSOC and regulates protein homeostasis. UCHL1 expression was markedly increased in HGSOC patient tumors and serous tubal intraepithelial carcinoma (HGSOC precursor lesions) and correlated with higher tumor grade and poor patient survival. UCHL1 inhibition reduced proliferation and invasion of HGSOC cells as well as significantly reduced the *in vivo* metastatic growth of the ovarian cancer xenografts. Transcriptional profiling of UCHL1 silenced HGSOC cells revealed down-regulation of genes implicated with proteasome activity along with the upregulation of endoplasmic reticulum (ER) stress-mediated genes. Silencing UCHL1 resulted in reduced expression of proteasome subunit alpha 7 (PSMA7) and acylaminoacyl peptide hydrolase (APEH) leading to a decrease in proteasome activity, accumulation of polyubiquitinated proteins, and reduced mTORC1 activity and protein synthesis. This induced ER-stress mediated pro-apoptotic factors, including ATF3 (activating transcription factor 3). In addition, the growth of HGSOC cells was significantly reduced upon silencing PSMA7 and APEH or inhibiting proteasome activity. Together, these results indicate that the UCHL1-PSMA7-APEH axis mediates the degradation of misfolded proteins, salvage amino acids for protein synthesis, and maintain protein homeostasis. This study highlights protein homeostasis as a therapeutic vulnerability in HGSOC and identifies UCHL1 and APEH inhibitors as novel therapeutic strategies.

Introduction

Dysregulated and uncontrolled proliferation is one of the hallmarks of cancer. To sustain the high proliferating state, cancer cells have high protein synthesis, which is intrinsically an error prone process [1]. It is estimated that up to 30% of newly synthesized misfolded proteins are degraded by the proteasome immediately after protein translation [1, 2]. Similarly, aberrant expression of mutants, stoichiometrically altered protein complexes and oxidatively damaged proteins in the onco-proteome create a proteotoxic state, if not efficiently removed [1, 3, 4].

Proteasomes are the prime cellular protein degradation machinery. Most cancer cells display high proteasome activity to alleviate proteotoxic stress response to avoid growth arrest, regulate cellular levels of proteins, like cell-cycle checkpoints or tumor suppressors, and to maintain the dynamic integrity of onco-proteome [5, 6]. Cancer cells adapt in various ways to enhance proteasome activity like upregulation of proteasome subunits, proteasome activators or proteasome assembly factors [7-10]. Moreover, deubiquitinating enzymes facilitate proteasomal degradation by substrate deubiquitination [1, 11, 12]. Treatment with pan-deubiquitinating enzyme inhibitor sensitizes cancer cells to proteotoxic stress under oxidative stress in absence of glutathione [13]. This suggests a broader role of deubiquitinating enzymes in mediating protein homeostasis. However, the role of specific deubiquitinating enzyme(s) in mediating proteostasis and proteasome activity remains unknown [13].

Proteasome inhibition has proven to be a successful therapy in hematological cancers, which largely depend on proteasomes for the removal of unwanted protein build-up and degradation of anti-survival signaling effectors to promote cancer growth [14, 15]. Interestingly, in solid tumors, a second-generation proteasome inhibitor (PI), Carfilzomib has started to show better outcomes in clinical trials due to precise specificity and sensitivity compared to Bortezomib [5]. Thus, it is critical to identify mechanisms that regulate proteasome activity in solid tumors in order to identify therapeutic targets upstream of proteasomes and to elucidate predictive factors and mechanisms that may lead to PI resistance. This would allow development of better combinational therapies.

High-grade serous ovarian cancer (HGSOC) is the most prevalent and deadliest subtype of ovarian cancer with a high case-to-fatality ratio [16-18]. Despite significant advances in the overall cancer diagnostics and therapeutics, early diagnosis and novel adjuvant treatments remain a challenge for HGSOC. HGSOC is a c-type malignancy, characterized by copy number variations, and germline or somatic mutations, including mutation in the tumor suppressor gene p53 [16]. Thus, understanding of mechanisms regulating proteostasis is an essential link to develop novel treatment strategies. Here, we conducted a systematic analysis of TCGA database and identified increased expression of deubiquitinating enzyme, ubiquitin carboxyl-terminal hydrolase 1 (UCHL1) in HGSOC patients. UCHL1 has been reported as both an oncogene [19-23] and tumor suppressor gene [24-27] in breast, colorectal and prostate cancer. The conflicting role of UCHL1 suggests its context-dependent role in cancer. However, UCHL1 is primarily a neuronal deubiquitinating enzyme, that constitutes about 1-2% of total brain proteins [28]. Loss of UCHL1 has been implicated in neurodegenerative diseases and reduced proteasome activity leading to accumulation of protein aggregates in the brain [29, 30]. However, the precise mechanism of regulation of proteasome activity by UCHL1 and its role in maintaining proteostasis in cancer remains unknown. We report that the UCHL1-PSMA7-APEH axis mediates proteasomal degradation of proteins and maintains protein homeostasis.

Materials and Methods

Cell lines and culture

HGSOC cell lines: Kuramochi, OVCAR4, OVCAR3, COV362, OVSAHO and OVCAR8 and non-HGSOC cell line: SKOV3, OVCAR5, HeyA8 and A2780 were cultured in 10% DMEM medium (Corning; cat#10-013-CV) supplemented with 1% non-essential amino acid and 1% vitamins and 1% penicillin/streptomycin (Corning) as described earlier [31]. Fallopian tube epithelial cells were obtained from Dr. Ronny Drapkin, University of Pennsylvania and were cultured in DMEM-Ham's F12 media (Corning) supplemented with 2% UltroserG (Crescent Chemical Company). Non-ciliated FT epithelial cells transfected with vector pWZL-mutant p53-R175H were obtained from Dr. Marcin Iwanicki and were cultured in WIT-Fo Culture Media from Live Tissue Culture Service Center, University of Miami [32]. Human primary mesothelial cells (HPMC) and fibroblasts isolated from the omentum of a healthy woman were obtained from Dr. Anirban Mitra, Indiana University and were grown in 10% DMEM. All cell lines were authenticated by short tandem repeat (STR) profiling and tested for mycoplasma contamination.

Patient samples

Human serous tubal intraepithelial carcinomas (STIC; n=3) were obtained from Dr. Ronny Drapkin, University of Pennsylvania. Frozen human serous ovarian cancer primary tumors and matched normal adjacent fallopian tube (FT) tissues were obtained from Indiana University Simon Cancer Center (IUSCC) tissue bank. The study was approved by the Institutional Regulatory Board of Indiana University (protocol numbers 1106005767 and 1606070934). Written consent was obtained from all the patients and only deidentified patient specimens were used. Tissue microarrays of HGSOC tumors with normal ovary (OV1502 and BC11012) and normal fallopian tube (UTE601) were purchased from US Biomax Inc and were processed at the same time.

HGSOC transcriptomic data analysis

UCHL1 expression across various cancer stages and tumor grades in HGSOC patients was analyzed in TCGA database using Oncomine gene browser [33]. Using KM plotter [34], progression free survival or overall survival was analyzed in HGSOC patients (n=1104) who had received chemotherapy after optimal or suboptimal debulking. Auto-select best cut-off and median expression cut-off was used for UCHL1 and PSMA7 respectively. Using OVMARK [35], disease free survival was analyzed in an *in-house* cohort of Molecular Therapeutics for Cancer, Ireland (MTCI) and GSE9899 (n=244). HGSOC patients with no residual tumors were analyzed and UCHL1 median expression was the cut-off. *TP53* mutation data (putative driver n=92, missense mutation n=143, and no mutation n=10) and UCHL1 expression data from HGSOC patients in TCGA database were retrieved from cBioportal [36].

Methylated DNA immunoprecipitation (MeDIP)

MeDIP was performed using Active Motif kit (Cat# 55009). Briefly, the genomic DNA was isolated from the ovarian cancer cell lines using DNeasy blood and tissue kit (Qiagen). Using a tip probe sonicator, DNA solution (20ng/µl) was sheared on ice for 3 pulses of 10 seconds at 30% amplitude with a 20 second pause between each pulse. The sheared DNA was visualized using Agilent TapeStation to ensure fragment size. DNA immuno-precipitation was performed using 5-methylcytosine antibody and control mouse IgG and DNA was eluted according to the manufacturer's protocol. MeDIP-qPCR for UCHL1 was performed in the input and MeDIP samples using primers fwd: ccgctagctgtttttcgtct, rev: ctcacctcggggttgatct. The data was analyzed as percent of input normalized to control IgG. Amplicons were resolved using 2% agarose gel. MeDIP for the positive control sample using ZC3H13 primers was run parallelly.

Chromatin immunoprecipitation (ChIP)

ChIP was carried out using ChIP-IT Express kit (Active Motif, cat# 53008). Briefly, cells were fixed for 10 mins using 1% methanol free formaldehyde (Fisher Scientific, cat# 28908) followed by Glycine-Stop Fix solution treatment for 5 mins. Cells were lysed in 1ml of ice-cold lysis buffer. Nuclei pellet was suspended in the shearing buffer and sonicated for 8 cycles of 30sec ON/OFF using Bioruptor Pico (Diagenode). The sheared chromatin was reverse-crosslinked and visualized using Agilent TapeStation to ensure fragments size. ChIP was performed according to the manufacturer protocol using anti-histone H3K4 trimethyl antibody (Abcam, ab8580) and control IgG. ChIP-qPCR for UCHL1 was performed using primers fwd: ccgctagctgtttttcgtct, rev: ctcacctcggggttgatct and the data was analyzed using $2^{-\Delta\Delta Ct}$ and normalized with input [37].

Cell proliferation and colony formation assay

Briefly, cells were plated in 96-well plate at a density of 2000 cells per well. After 4 days cells were treated with 20µl of MTT solution (5mg/ml) and were incubated at 37°C for 3h. The reduction of MTT into purple color formazan by the metabolically active cells was spectrophotometrically measured at 560nm and was adjusted for the background absorbance at 670nm. For the colony formation assay, cells were seeded at a density of 1000 cells per well in a 6-well plate. The colonies were allowed to grow for 8-10 days, were fixed using 4% paraformaldehyde and stained with 0.05% crystal violet solution. The colonies were imaged and counted using ImageJ.

Fallopian tube epithelial cells spheroid culture and ethidium bromide (EtBr) assay

Fallopian tube non-ciliated epithelial (FNE) cells expressing mutant p53 R175H and green-fluorescence protein (GFP) (thereafter referred as FNE-mp53^{R175H}) were seeded in ultra low-adhesion plates (Corning). To support basement membrane adhesion, 2% Matrigel was added to the suspended culture after 24hrs. On the fifth day post Matrigel addition, three-dimensional (3D) structures of FNE-mp53^{R175H} cells were treated with DMSO or UCHL1 inhibitor, LDN 57444 (1 and 10 mM). Subsequently, after 5 days cellular clusters were treated with 2µM EtBr (Molecular Probes) and were imaged and EtBr incorporation was measured as number of pixels (red channel within cellular clusters as described earlier [32].

Invasion through three-dimensional organotypic cell culture

Invasion of HGSOC cells through the 3D culture of omental cells was studied as described earlier [38]. Briefly, $2x10^5$ fibroblasts with collagen I and $2x10^6$ human primary mesothelial cells (HPMC) isolated from the omentum of a healthy woman were seeded in a fluoroblock transwell insert (8µm pore size, BD Falcon). Next day, $2x10^5$ UCHL1 silenced or unsilenced OVCAR3 (RFP labelled) and Kuramochi (GFP labelled) cells in 200µl of serum-free DMEM were plated over the omental cells. Subsequently, the insert was placed in a well of 24-well plate containing 700µl of 10% DMEM. Cells were allowed to invade for 16h and were fixed with 4% paraformaldehyde. The invaded cells were imaged (5 fields/insert) and counted.

Proteasome activity and Acylaminoacyl-peptide hydrolase (APEH) activity

The chymotrypsin-like protease activity was measured using fluorogenic substrate LLVY-R110 (Sigma-Aldrich; cat# MAK172) as per manufacturer's protocol and as described earlier [39]. Total protein (50µg) from fresh cell lysate or tissue homogenates in even volumes (90 µl) was incubated with 100µl of proteasome assay buffer containing fluorogenic substrate LLVY-R110 at 37°C. R110 cleavage by proteasomes was measured at 525nm with excitation at 490nm. Fluorescence intensity was normalized with the fluorescence of blank well. APEH activity was measured using chromogenic substrate acetyl-Ala-pNa (Bachem) [40]. Total protein (45µg) in even volume (100 µl) in 50mM Tris-HCl buffer pH7.5 was preincubated at 37°C for 2mins. Thereafter, 1mM Ac-Ala-pNA was added and the release of p-nitroaniline was measured at 410nm.

Immunoblotting

Immunoblotting was performed using standard protocol as described earlier [38]. Briefly, total proteins were extracted using NP-40 lysis buffer supplemented with 0.2mM phenylmethylsulfonyl fluoride, 10mM N' ethylmalamide, protease and phosphatase inhibitors cocktails (Millipore). Proteins were resolved by 4-20% gradient SDS-PAGE. Following antibodies were used: UCHL1 (13179, Cell Signaling), UCHL1 (MAB6007, R&D Systems), actin-HRP (Sigma), PSMA7 (cat# PA5-22289; Invitrogen), ATF3 (cat# 33593; Cell signaling), APEH (cat# 376612; SantaCruz Biotechnology). The band density was determined by ImageJ.

Cell treatments

Ovarian cancer cells were plated at a 50% confluency and were treated with 5-Aza-2′-deoxycytidine (5AzaDC; Sigma-Aldrich; cat# A3656; 5μM; 48h) to allow its incorporation into the DNA of the dividing cells [41]. In separate experiments, Nutlin 3 (Sigma-Aldrich; cat# N6287) or LDN57444 (EMD Millipore; cat# 662086) or Carlfilzomib (cat# S2853, Selleck Chemicals) were treated at the indicated dose and timepoints.

Transfection and Tranduction

HGSOC cells were transfected with ON-TARGET Plus four silencing RNA for UCHL1 (cat# L-004309-00-0010) or PSAM7 (cat# L-004209-00-0010) or APEH (cat# L-005785-00-0010) and scramble control (cat# D-001810-10-05) from Dharmacon using TransITX2 (Mirus Bio; cat#MIR6000) according to the manufacturer's protocol. HGSOC cells were transduced with control or UCHL1 shRNA lentiviral virus particles (Santacruz Biotechnology; cat# sc-108080 and sc-42304-V) using TransDux™ MAX (System Biosciences; cat#LV860A-1).

Mouse xenograft model

Mouse xenograft model of HGSOC was used as described earlier [42]. Briefly, 6-weeks old female athymic nude mice (Envigo) were intraperitoneally injected with $5x10^6$ OVCAR8 cells. After 10 days mice were randomized into two groups (n=10 mice/group) and were intraperitoneally injected with LDN57444 (1mg/Kg) or 25% DMSO thrice/week for 5 weeks. The study was approved by the Institutional Biosafety Committee and Institutional Animal Care and Use Committee.

Immunohistochemistry (IHC)

IHC was performed at IU Health's pathology laboratory. Briefly, slides were baked at 60°C for 30 minutes before standard deparaffinization procedure followed by blocking of endogenous peroxides and biotin. Antigen retrieval was performed using 10mM citrate buffer, pH6.0 at 95°C followed by 1h blocking and incubation with pre-optimized primary anti-UCHL1 or anti-p53 antibodies (1:200 dilution). TMA slides were digitally scanned by Aperio ScanScope CS slide scanner (Aperio Technologies) and staining was quantified in three intensities ranges: weak – 0 to 100, positive – 100 to 175 and strong – 175 to 220. TMA slides were also hand-scored by Dr. George Sandusky as 1 being weak expression, 2 moderate, 3 strong and 3+ very strong.

Assay for transposase-accessible chromatin (ATAC) sequencing

Assay for transposase-accessible chromatin with high-throughput sequencing was performed at Center for Medical Genomics, Indiana University School of Medicine using Tagment DNA TDE1 enzyme and Nextera DNA Flex Library Prep kit (Illumina cat#15027866 and 15027865). Briefly, $1x10^5$ OVCAR3 and SKOV3 cells were lysed in a non-ionic detergent to yield pure nuclei. The chromatin was fragmented and simultaneously tagmented with the sequencing adaptor using Tn5 transposase to generate ATAC-seq libraries, which were sequenced on NextSeq 500 (Illumina) with NextSeq75 High Output v2 kit (Illumina, cat# FC-404-2005). Raw fastq files were aligned to

human GRCH38 genome by using bowtie 2 [43]. MACS2 and ENCODE standardized pipeline and parameters were utilized for peak detection [44]. Peaks on the promoter region of UCHL1 gene were plotted using UCSC genome browser [45].

RNA isolation, Realtime PCR and RNA sequencing

Total RNA from cell lines and patient tumors was extracted using miRNeasy mini kit (Qiagen; cat#217004) and cDNA was prepared using high capacity reverse transcription Kit (Applied Biosystems; cat#4368814). Real-time PCR was performed using TaqMan gene expression assays for UCHL1, TP53, PSMA7, APEH, CDKN1A (p21), HMOX1, ATF3. β-actin and tata-box binding protein were used as endogenous control. For RNA-sequencing, 1 µg of total RNA was used for library preparation using TruSeq Stranded mRNA kit (Illumina, cat# RS-122-2103) after rRNA depletion using Ribo-Zero plus (Illumina; cat#20037135). RNA-sequencing was performed using NextSeq75 High Output v2 kit and NextSeq 500 (Illumina; cat# FC-404-2005). Using TruSeq 3' SE adaptor sequence AGATCGGAAGAGCACACGTCTGAACTCCAGTCAC, RNA-seq reads were trimmed and then were mapped to the gene regions in strand specific manner using htseq-count (version 0.5.4p1) [46]. Differentially expressed genes at 5% FDR with at least two-fold change were called using DESeq2 ver.1.12.3 as described earlier [47].

Statistical analysis

All results are expressed as mean ± SD from three biological repeats unless otherwise stated. Statistical significance between two groups was calculated using 2-tailed Student's t test. Statistical significance was calculated using one-way ANOVA in the experiments involving three groups. Box and whiskers plots were generated using Prism 8.0. The box plot boundaries represent the upper and lower quartiles, horizontal line represent the median value, and the whiskers represent the minimum and maximum values. Logrank test was used to determine significance between Kaplan Meier survival curves using KM plotter and OVMARK. A *P* value less than 0.05 was considered significant.

Results

UCHL1 expression is an early event in HGSOC and associates with poor prognosis

Our analysis of TCGA data revealed that UCHL1 is a frequently overexpressed gene in HGSOC patients. UCHL1 mRNA levels were significantly high in primary and recurrent tumors compared to normal ovaries (Figure 1A). Moreover, UCHL1 expression was markedly elevated in HGSOC patients with advanced-stage and higher-grade tumors compared to grade 1 and stage 1 tumors, respectively (Figures 1B and 1C). To confirm these results at the protein level, we performed UCHL1 immunohistochemical (IHC) staining in tissue microarrays of HGSOC tumors, including normal ovary and normal fallopian tube (FT) tissues. In comparison to normal tissues, UCHL1 expression was significantly higher in HGSOC tumors (Figures 1D and 1E). UCHL1 staining was positive in 78.4% (69 out of 88) of patients and its expression was high in 59.1% (52 out of 88) of patients, whereas its expression was negligible or low in the normal fallopian tube (FT) and ovary. Furthermore, aberrant expression of UCHL1 mRNA and protein levels were also observed in 8 out of 9 primary tumors compared to their matched normal adjacent FT (Figure 1F, paired samples). These results confirm that UCHL1 expression is upregulated in HGSOC. To confirm if UCHL1 expression is an early event in HGSOC, we performed UCHL1 IHC staining in serous tubal intraepithelial carcinoma (STIC). HGSOC is known to be originated from the lesions in FT known as STIC. *TP53* mutations are an early event in the development of STIC and the presence of identical *TP53* mutations in STIC and concurrent HGSOC established their clonal relationship [48]. UCHL1 levels were significantly elevated in the epithelial cells and the associated invasive

carcinoma of STIC along with diffused nuclear staining of mutant p53 (Figure 1G), while the staining was absent in p53-negative regions and normal human FT (Figures 1G and S1). Next, we analyzed the transcriptomic datasets of HGSOC patients to understand the prognostic significance of UCHL1 using the Kaplan Meier plotter and OVMARK. Survival analysis revealed a significant association of high UCHL1 levels with poor progression-free survival of HGSOC patients after chemotherapy and debulking (Figure 1H) and with poor disease-free survival after optimal debulking in HGSOC patients from GSE9899 and patients from the *in-house* cohort of Molecular Therapeutics for Cancer, Ireland (Figure 1J). These results indicate that UCHL1 overexpression is crucial for HGSOC growth and predicts poor patient prognosis.

Epigenetic upregulation of UCHL1 in HGSOC

UCHL1 is known to be a silenced as well as an overexpressed gene in several cancers such as breast and colorectal cancers [19, 20, 24, 25]. Thus, the regulation of its expression in cancer remains elusive. We examined the expression of UCHL1 in a panel of ovarian cancer cell lines characterized [49] as HGSOC and non-HGSOC cell lines. Compared to non-HGSOC cell lines, UCHL1 mRNA and protein levels were significantly higher in HGSOC cell lines (Figure 2A). Strikingly, elevated UCHL1 levels in HGSOC cell lines varied across different *TP53* mutations and mutant p53 levels in these cell lines (Figures 2A and 2B). In contrast, in the non-HGSOC cell lines, UCHL1 expression was low or completely absent in cells with WT p53 or p53-null respectively (Figures 2A and 2B). We performed methylated DNA immunoprecipitation (MeDIP) using 5-methylcytosine (5MC) antibody in Kuramochi and OVCAR3 (HGSOC) and HeyA8 and OVCAR5 (non-HGSOC) cells. No enrichment of methylated DNA in the UCHL1 promoter was observed in HGSOC cells, while significant enrichment was observed in non-HGSOC cell lines (Figure 2C and S2A). Similarly, our ATAC-seq data revealed open chromatin at the UCHL1 gene promoter (chromosome 4; region 41257000-41258000; exon 1 to exon 3) in OVCAR3, unlike the non-HGSOC, SKOV3 cells (Figure 2D). Confirming our ATAC-seq results, chromatin immunoprecipitation (ChIP) assay using the H3K4 trimethylated antibody revealed enhanced enrichment of H3K4 trimethylated chromatin in the UCHL1 promoter in HGSOC cells, OVCAR3 and OVCAR4 (Figure 2E). However, no such enrichment of H3K4 trimethylated chromatin was observed in SKOV3 (Figure 2E). Together, these results confirmed that unmethylated CpG islands in UCHL1 promoter supports high UCHL1 expression in HGSOC. To further confirm these results, we treated HGSOC and non-HGSOC cell lines as in Figure 2A with DNA methyltransferase inhibitor, 5-Aza-2'Deoxycytidine (5-Aza-DC). No change in UCHL1 expression was observed in HGSOC cell lines upon treatment with 5-Aza-DC (Figure 2F), while UCHL1 expression was increased many folds in non-HGSOC cell lines (Figure 2G). These results demonstrate that partial or complete epigenetic silencing of the UCHL1 gene in non-HGSOC, as reported previously [50]. Similarly, 5-Aza-DC treatment in normal human fallopian tube epithelial (FTE) cells showed a significant increase in UCHL1 levels (Figure S2B). Collectively, these results demonstrate that epigenetic upregulation of UCHL1 is HGSOC-specific.

UCHL1 regulates HGSOC growth *in vitro* and *in vivo*

We knocked down UCHL1 expression in HGSOC cell lines: Kuramochi, OVCAR3, OVCAR4 and OVSAHO. Cellular proliferation (Figure 3A) and clonogenic growth (Figures 3B and 3C) of HGSOC cell lines were significantly reduced upon silencing UCHL1 (Figure S3A). Omentum is the most favorable site for HGSOC metastasis. To mimic the omental metastasis, we utilized a three-dimensional (3D) organotypic cell culture of omental mesothelial cells and fibroblasts [38] in a transwell insert (Figure S3B). The invasion of UCHL1 silenced Kuramochi (GFP labeled) and OVCAR3 (RFP labeled) cells through the omental 3D culture was significantly reduced in

comparison to the unsilenced controls (Figure 3D). Prolonged anchorage-independent survival (as the floating cells in the ascites) is crucial for the metastatic spread and exemplify spread of HGSOC from the precursor lesions in FT. Prolonged anchorage-independent survival of non-ciliated FT epithelial (FNE) cells overexpressing mutant p53 variant R175H ($FNE^{mutp53\text{-}R175H}$) has been reported [32]. Increased UCHL1 expression was seen in $FNE^{mutp53\text{-}R175H}$ cells (Figure S3C). Therefore, we treated the organoid culture of $FNE^{mutp53\text{-}R175H}$ with the UCHL1 inhibitor, LDN57444 (LDN; 1 and 10μM, 5 days) and quantified the suspension culture-associated cell death using ethidium bromide (EtBr) incorporation. Compared to untreated cells, LDN-treated $FNE^{mutp53\text{-}R175H}$ cells showed reduced GFP expression and increased EtBr intercalation into DNA due to cell death associated nuclear membrane fracture (Figures 3E). Supporting this data, LDN treatment in OVCAR5 cells, which do not express UCHL1 (Figure 2A), showed no effect of LDN57444 on cellular proliferation (Figure S3D), indicating the specificity of LDN57444 for UCHL1. Collectively, the data demonstrate that UCHL1 is critical for HGSOC growth and metastasis. To confirm these results on *in vivo* tumor growth, we used a mouse xenograft model of ovarian cancer metastasis (Figure S3E). UCHL1 inhibitor LDN57444 (LDN) treatment resulted in significantly smaller and fewer tumors (metastatic nodules) compared to tumors in the vehicle control group (Figures 3F and 3G). Moreover, the overall weight of the surgically resected tumors was significantly less in the LDN-treated mice compared the control mice (Figures 3H and 3I). Histology of tumors from LDN and vehicle control groups were similar on hematoxylin and eosin (H&E) staining (Figure S3F). Similarly, *in vitro* treatment of LDN as well as UCHL1 knockdown in OVCAR8 cells exhibited significant reduction in the cell growth (Figures S3G and S3H). Collectively, the data confirm that UCHL1 inhibition affects HGSOC tumor growth and metastasis.

UCHL1 knockdown associates with the activation of unfolded protein response and impaired proteasome activity.

Since the dubs specificity for their target remains questionable, we performed the transcriptional profiling in the UCHL1 silenced Kurmamochi cells to identify the potentially dysregulated pathways or molecular mechanisms after UCHL1 knockdown. A total of 1004 genes were significantly differentially expressed in Kuramochi cells upon silencing UCHL1 with a 1% false discovery rate. Analysis of top 35 dysregulated genes (Figure 4A) revealed the upregulation of stress-induced genes, including heat-shock factor 1 target gene HMOX1 (Heme Oxygenase 1) and endoplasmic reticulum (ER) stress-induced gene, ATF3 (activating transcription factor 3). Volcano plot of differentially expressed genes revealed activation of unfolded protein response (UPR) as measured by the upregulation of DDIT3 (CHOP), ATF4, ATF3, GADD35, HSP40 [13] (Figure 4B). In contrast to the upregulation of proteotoxic and ER stress-induced genes, the genes implicated with proteasome activity were the top down-regulated genes in our RNA-seq data (Figure 4A). The expression of proteasome subunit alpha 7 (PSMA7) and acylaminoacyl peptide hydrolase (APEH) was significantly reduced upon silencing UCHL1 in our RNA-seq data (Figure 4A) and subsequent qPCR validation in HGSOC cell lines (Figure 4C). Inhibition of proteasome activity has been associated with the induction of terminal UPR [51, 52]. These results indicate that UCHL1 inhibition results in impaired degradation of proteins leading to activation of the ER stress response.

PSMA7 and APEH mediates proteasome activity and HGSOC growth

Proteasome subunit alpha 7 (PSMA7) proteasome isoform has been associated with enhanced resistance to stress in yeast and mammalian cells [53]. To evaluate the significance of PSMA7 in HGSOC, we analyzed PSMA7 expression in HGSOC patient tumors. Our analysis of TCGA database revealed increased expression of PSMA7 in HGSOC tumors (Figure 5A) and its

correlation with poor overall survival of HGSOC patients after optimal debulking (Figure 5B). Silencing PSMA7 demonstrated significantly reduced chymotrypsin-like proteasome activity and 20S proteasome levels in HGSOC cells, Kuramochi, and OVCAR4 (Figures 5C and 5D), leading to the accumulation of polyubiquitinated proteins (Figure 5E). Consistent with these findings, cellular proliferation and clonogenic growth of HGSOC cells were significantly reduced upon silencing PSMA7 (Figures 5F and 5G). These results indicate that PSMA7-mediated proteasome activity promotes HGSOC growth. Similarly, the activity of cytosolic enzyme, acylaminoacyl peptide hydrolase (APEH) is associated with increased proteasome activity [40]. APEH catalyzes the removal of *N*-acetylated amino acid from the acetylated peptides leading to the release of free amino acid. The activity of APEH possibly disrupts the negative feedback inhibition of proteasomal activity caused by the accumulation of *N*-acetylated peptides after proteasomal degradation of proteins [40]. The expression of APEH was significantly high in HGSOC tumors compared to normal ovaries in TCGA database (Figure 5H). Moreover, APEH activity and expression were significantly reduced in UCHL1 silenced HGSOC cells (Figures 5I, 5J, and 5K), and reduced APEH activity demonstrated reduced chymotrypsin-like proteasome activity in HGSOC cells (Figure 5L). Supporting these results, cellular proliferation and clonogenic growth of HGSOC cells were significantly reduced upon silencing APEH (Figures 5M and 5N). Collectively, these results demonstrate that the UCHL1-PSMA7-APEH axis mediates proteasome activity and HGSOC growth.

UCHL1 inhibition induces terminal stress response and attenuates mTORC1 activity

The above results led us to hypothesize that the vulnerability of HGSOC cells to reduced proteasome activity, maybe, at least in part due to proteotoxic stress. Inhibition of proteasomal degradation of proteins induces proteotoxicity leading to activation of terminal UPR and attenuates protein translation [51, 54, 55]. Consistent with this hypothesis, polyubiquitinated proteins accumulated following UCHL1 silencing and treatment with UCHL1 inhibitor, LDN57444 in HGSOC cells, Kuramochi, and OVCAR4 (Figures 6A and 6B). These results were supported by reduced proteasome activity in LDN57444-treated xenograft tumors (Figure 6C) and dose-dependent decrease in cellular proliferation of Kuramochi cells upon treatment with second-generation proteasome inhibitor, carfilzomib (Figure 6D). Furthermore, UCHL1 inhibition resulted in reduced mTORC1 (mammalian target of rapamycin complex 1) activity and protein synthesis as evidenced by decreased phosphorylated levels of two mTORC1 substrates, ribosomal protein S6 (S6), and the eukaryotic initiation factor 4E- binding protein (4EBP1) in UCHL1 silenced Kuramochi cells (Figure 6E). In contrast, the expression of ER stress-induced proteins, ATF4, ATF3, and pro-apoptotic protein CHOP was increased while the expression of anti-apoptotic protein BCL2 was decreased (Figure 6E). These results indicate that UCHL1 inhibition results in impaired protein degradation, leading to the accumulation of proteins resulting in attenuation of protein synthesis and activation of terminal UPR. Collectively, the data demonstrate that the UCHL1-PSMA7-APEH axis mediates proteasomal degradation of misfolded or damaged proteins and maintains protein homeostasis to promote HGSOC growth (Figure 6F).

Discussion

Accumulating evidence has revealed the crucial roles of deubiquitinating enzymes in cancer-associated signaling and have identified them as prognostic markers based on correlations with tumor size and cancer staging [56, 57] . We have now shown the role of deubiquitinating enzyme, UCHL1 in mediating proteasome activity and the importance of the proteostasis network in HGSOC growth and survival. This study provides novel insights into HGSOC survival mechanisms by maintaining proteostasis via the UCHL1-PSMA7-APEH-proteasome axis. It also

highlights the epigenetic upregulation of UCHL1 in HGSOC harboring mutant p53 variants. Consistent with these findings, treatment with the UCHL1 inhibitor, LDN57444 retarded the growth of metastatic tumors *in vivo*.

Due to the lack of mechanistic studies demonstrating the regulation of proteasome activity or pathways supporting proteostasis in HGSOC, the use proteasome inhibitors or inhibitors from the proteostasis network has been limited in HGSOC interventions. For the first-time, we report that UCHL1-mediates proteasome activity in cancer via transcriptional upregulation of proteasome subunit -PSMA7 and cytosolic peptide hydrolase -APEH, which in turn results in increased chymotrypsin like proteasome activity and 20S proteasome levels in HGSOC. Upregulation of proteasome subunit, PSMA3 has been associated with increased proteasome activity in cancer and resistance to proteasome inhibitor [7]. Though, role of PSMA7 in evolutionarily conserved proteasome isoform with increased proteasome activity has been reported [53]. Deubiquitinating enzymes are important regulators of gene transcription [58]. Ataxin 3 is a deubiquitinating enzyme as well as transcriptional co-repressor, which is involved in protein homeostasis [59]. It is possible that UCHL1 itself acts as a transcriptional co-activator or indirectly co-operates with another transcription factor. Moreover, cancer-associated transcription factors, including mutant p53, have recently been shown to upregulate proteasome machinery [39]. Increased proteasome activity is a feature of several malignancies, as cancer cells depend on proteasome activity to alleviate proteotoxicity and remove access of misfolded or damaged proteins [6, 15]. Proteasome function is also important to maintain the dynamic integrity of onco-proteome and to degrade tumor suppressors or oncogenic signaling effectors [6, 15]. Our data shows that UCHL1-mediated increase in proteasome activity mediates protein homeostasis in HGSOC. Reduced proteasome activity resulted in abrogated protein degradation and proteasome overload leading to protein accumulation and proteotoxicity. These findings are supported by our RNA-seq data showing increased expression of stress-induced genes upon silencing of UCHL1. Furthermore, for the first time we report that UCHL1 inhibition leads to activation of HSF1 and induction of HSF1-induced genes; HMOX1 and ATF3 [60, 61]. ATF3 is a marker of unfolded protein response and is induced to promote cell survival under cellular stress conditions. ATF3 knockdown inhibits proteasome inhibitor-induced cell death [62, 63]. In contrast, ATF3 is also known to suppress expression of inflammatory cytokines to impair repair response [60]. Though, ATF3 suppresses mutant p53-induced NFKB2 expression [64], its role in mutant p53-HSF1 response is unclear. Similarly, HMOX1 is induced under various stresses and helps in maintaining cellular homeostasis [61]. Moreover, HSF1 activation is a key step in the management of the proteotoxic stress response, and proteasome inhibition induces HSF1 in response to accumulation of proteins [65]. Thus, we demonstrate that UCHL1-mediated proteasome activity in HGSOC, which is a c-type malignancy, is crucial to avoid proteotoxicity and growth arrest. In solid tumors, such as lung, pancreas, breast and head and neck cancer, second generation proteasome inhibitor, carfilzomib has shown better results due to greater selectivity, inhibitory potency for proteasome subunits and an improved clinical safety profile than Bortezomib [5]. Continued interest in exploring the potential of proteasome inhibitors for treatment of solid tumors is supported by our findings.

We identified that UCHL1 overexpression in HGSOC supports metastatic tumor growth and correlates with disease progression and poor patient prognosis. These findings are consistent with the other studies reporting UCHL1 as an oncogene in cancer. To better understand the role of UCHL1 as a prognostic marker for cancer and to further develop diagnostic and therapeutic strategies targeting UCHL1, we studied the context-dependent role of UCHL1 in cancer and identified the underlying mechanism that regulates its expression. Our data indicate that UCHL1 expression levels were elevated in HGSOC tumors, and cell lines harboring *TP53* mutations. We further established a link between mutant p53 and UCHL1 overexpression based on several correlating observations. Interestingly, UCHL1 expression was upregulated in the mutant p53-

positive regions of STIC, identified by strong nuclear mutant p53 staining while the expression was absent in mutant p53-negative regions. Similarly, UCHL1 levels were higher in HGSOC patients with high p53 expression levels and missense mutations and a correlation (r=0.2) was observed. Furthermore, we reported that in mutant p53 background, UCHL1 expression is epigenetically upregulated due to decreased activity of DNMTs on the UCHL1 promoter, influenced by open chromatin at UCHL1 promoter, H3K4 methyltransferases activity and enhanced H3K4 trimethylation. DNMTs have no gene specificity and are largely recruited by histone methyltransferases [66]. Though, expression of H3K4 methyl transferases, MLL1/2 and 3 (KMT2A, KMT2B, KMT2C) is higher in HGSOC patient tumors compared to normal ovary in TCGA database (data not shown), details of specific SET1/compass H3K4 methyl transferase and potential play of mutant p53 in the epigenetic upregulation of UCHL1 remains unknown. However, transcriptional upregulation of H3K4 histone methyltransferases by GOF mutant p53 variants have been reported in breast cancer [37]. About 96% of HGSOC patients have mutated p53, varying from missense mutations to truncated and in-frame deletions. Accumulating evidences suggest the role for mutant p53-HSF1-HSP (heat shock proteins) in mediating proteotoxic stress response and rendering cancer cell more resistant to proteotoxic stress [67]. In support of this, transcriptional upregulation of proteasomal machinery by the mutant p53-NRF2 axis and increase proteasome activity has also been reported in breast cancer [39]. Together, these evidences supported the context-dependent upregulation of UCHL1 in HGSOC to mediate protein homeostasis via regulating proteasome activity. Defining a mass-spectrometry based target of UCHL1, can potentially reveal another layer of mechanistic regulation of proteostasis in HGSOC and a link between UCHL1 and mutant p53 in the proteostasis network.

The human protein atlas shows that UCHL1 protein levels are high in brain, but it is not present in other tissues except for pancreas, kidney, colon, testis and soft tissues. Yet, UCHL1 overexpression has been reported in human cancers of breast, lung, prostate and myeloma. UCHL1 expression in cancer could be an adaptive mechanism to support cancer growth. It has been demonstrated that UCHL1 regulates malignant growth through interactions with HIF-1, cyclin B1 and β-catenin by mediating their cellular stability or nuclear levels [20, 68, 69]. Our study compliments these reports, as increased proteasomal degradation have been reported for Von Hippel Lindau, an E3 ligase for HIF-1α, and negative regulators of Wnt-β-catenin signaling, Dishevelled and Adenomatous Polyposis Coli (APC) [70, 71]. In neurodegenerative diseases, like Alzheimer's disease, loss of UCHL1 has been implicated in accumulation of amyloid β aggregates through decreased 26S proteasomal activity by an unknown mechanism. Therefore, our novel findings could potentially be applied as therapeutic strategies upstream of proteasomes or in combination with a proteasome inhibitor. UCHL1 inhibitor, LDN57444 has shown significant effects on solid tumor growth [68] and similar results were observed in our *in vivo* and organoid culture studies. This suggests the use of LDN57444 in other models or further development of pharmaceutical grade compound. Various small-molecule deubiquitinating enzyme inhibitors are emerging as a therapeutic modality for the treatment of cancer, such as USP14 inhibitor, VLX1570 in myeloma, NCT02372240. In addition, our study revealed another potential inhibitor, such as the APEH inhibitor, conjugated linoleic acid (t10,C12 CLA) [40], which can be tested to target the UCHL1-PSMA7-APEH-proteasome axis in HGSOC. Thus, our study provides a number of potential targets to clinically exploit proteostasis in cancer cells or HGSOC.

References

1. Guang, M.H.Z., et al., *Targeting Proteotoxic Stress in Cancer: A Review of the Role that Protein Quality Control Pathways Play in Oncogenesis.* Cancers (Basel), 2019. **11**(1).
2. Schubert, U., et al., *Rapid degradation of a large fraction of newly synthesized proteins by proteasomes.* Nature, 2000. **404**(6779): p. 770-4.
3. Mantovani, F., L. Collavin, and G. Del Sal, *Mutant p53 as a guardian of the cancer cell.* Cell Death Differ, 2019. **26**(2): p. 199-212.
4. Reeg, S., et al., *The molecular chaperone Hsp70 promotes the proteolytic removal of oxidatively damaged proteins by the proteasome.* Free Radic Biol Med, 2016. **99**: p. 153-166.
5. Roeten, M.S.F., J. Cloos, and G. Jansen, *Positioning of proteasome inhibitors in therapy of solid malignancies.* Cancer Chemother Pharmacol, 2018. **81**(2): p. 227-243.
6. Naujokat, C. and S. Hoffmann, *Role and function of the 26S proteasome in proliferation and apoptosis.* Lab Invest, 2002. **82**(8): p. 965-80.
7. Xu, H., et al., *Exosome-Transmitted PSMA3 and PSMA3-AS1 Promote Proteasome Inhibitor Resistance in Multiple Myeloma.* Clin Cancer Res, 2019. **25**(6): p. 1923-1935.
8. Ali, A., et al., *Differential regulation of the REGgamma-proteasome pathway by p53/TGF-beta signalling and mutant p53 in cancer cells.* Nat Commun, 2013. **4**: p. 2667.
9. Chondrogianni, N., et al., *Overexpression of proteasome beta5 assembled subunit increases the amount of proteasome and confers ameliorated response to oxidative stress and higher survival rates.* J Biol Chem, 2005. **280**(12): p. 11840-50.
10. Zhang, X., et al., *MicroRNA-101 Suppresses Tumor Cell Proliferation by Acting as an Endogenous Proteasome Inhibitor via Targeting the Proteasome Assembly Factor POMP.* Mol Cell, 2015. **59**(2): p. 243-57.
11. Koulich, E., X. Li, and G.N. DeMartino, *Relative structural and functional roles of multiple deubiquitylating proteins associated with mammalian 26S proteasome.* Mol Biol Cell, 2008. **19**(3): p. 1072-82.
12. Sun, C., et al., *Elevation of proteasomal substrate levels sensitizes cells to apoptosis induced by inhibition of proteasomal deubiquitinases.* PLoS One, 2014. **9**(10): p. e108839.
13. Harris, I.S., et al., *Deubiquitinases Maintain Protein Homeostasis and Survival of Cancer Cells upon Glutathione Depletion.* Cell Metab, 2019. **29**(5): p. 1166-1181 e6.
14. Kaplan, G.S., et al., *Proteasome inhibitors in cancer therapy: Treatment regimen and peripheral neuropathy as a side effect.* Free Radic Biol Med, 2017. **103**: p. 1-13.
15. Goy, A. and F. Gilles, *Update on the proteasome inhibitor bortezomib in hematologic malignancies.* Clin Lymphoma, 2004. **4**(4): p. 230-7.
16. Bowtell, D.D., et al., *Rethinking ovarian cancer II: reducing mortality from high-grade serous ovarian cancer.* Nat Rev Cancer, 2015. **15**(11): p. 668-79.
17. Lengyel, E., *Ovarian cancer development and metastasis.* Am J Pathol, 2010. **177**(3): p. 1053-64.
18. Siegel, R.L., K.D. Miller, and A. Jemal, *Cancer Statistics, 2017.* CA Cancer J Clin, 2017. **67**(1): p. 7-30.
19. Schroder, C., et al., *Prognostic relevance of ubiquitin C-terminal hydrolase L1 (UCH-L1) mRNA and protein expression in breast cancer patients.* J Cancer Res Clin Oncol, 2013. **139**(10): p. 1745-55.
20. Zhong, J., et al., *UCHL1 acts as a colorectal cancer oncogene via activation of the beta-catenin/TCF pathway through its deubiquitinating activity.* Int J Mol Med, 2012. **30**(2): p. 430-6.
21. Leiblich, A., et al., *Human prostate cancer cells express neuroendocrine cell markers PGP 9.5 and chromogranin A.* Prostate, 2007. **67**(16): p. 1761-9.

22. Hussain, S., et al., *UCHL1 is a biomarker of aggressive multiple myeloma required for disease progression.* Oncotarget, 2015. **6**(38): p. 40704-18.
23. Bedekovics, T., et al., *UCH-L1 is induced in germinal center B cells and identifies patients with aggressive germinal center diffuse large B-cell lymphoma.* Blood, 2016. **127**(12): p. 1564-74.
24. Xiang, T., et al., *The ubiquitin peptidase UCHL1 induces G0/G1 cell cycle arrest and apoptosis through stabilizing p53 and is frequently silenced in breast cancer.* PLoS One, 2012. **7**(1): p. e29783.
25. Okochi-Takada, E., et al., *Silencing of the UCHL1 gene in human colorectal and ovarian cancers.* Int J Cancer, 2006. **119**(6): p. 1338-44.
26. Ummanni, R., et al., *Ubiquitin carboxyl-terminal hydrolase 1 (UCHL1) is a potential tumour suppressor in prostate cancer and is frequently silenced by promoter methylation.* Mol Cancer, 2011. **10**: p. 129.
27. Yu, J., et al., *Epigenetic identification of ubiquitin carboxyl-terminal hydrolase L1 as a functional tumor suppressor and biomarker for hepatocellular carcinoma and other digestive tumors.* Hepatology, 2008. **48**(2): p. 508-18.
28. Setsuie, R. and K. Wada, *The functions of UCH-L1 and its relation to neurodegenerative diseases.* Neurochem Int, 2007. **51**(2-4): p. 105-11.
29. Lombardino, A.J., et al., *Replaceable neurons and neurodegenerative disease share depressed UCHL1 levels.* Proc Natl Acad Sci U S A, 2005. **102**(22): p. 8036-41.
30. Graham, S.H. and H. Liu, *Life and death in the trash heap: The ubiquitin proteasome pathway and UCHL1 in brain aging, neurodegenerative disease and cerebral Ischemia.* Ageing Res Rev, 2017. **34**: p. 30-38.
31. Haley, J., et al., *Functional characterization of a panel of high-grade serous ovarian cancer cell lines as representative experimental models of the disease.* Oncotarget, 2016. **7**(22): p. 32810-20.
32. Iwanicki, M.P., et al., *Mutant p53 regulates ovarian cancer transformed phenotypes through autocrine matrix deposition.* JCI Insight, 2016. **1**(10).
33. Rhodes, D.R., et al., *ONCOMINE: a cancer microarray database and integrated data-mining platform.* Neoplasia, 2004. **6**(1): p. 1-6.
34. Gyorffy, B., A. Lanczky, and Z. Szallasi, *Implementing an online tool for genome-wide validation of survival-associated biomarkers in ovarian-cancer using microarray data from 1287 patients.* Endocr Relat Cancer, 2012. **19**(2): p. 197-208.
35. Madden, S.F., et al., *OvMark: a user-friendly system for the identification of prognostic biomarkers in publically available ovarian cancer gene expression datasets.* Mol Cancer, 2014. **13**: p. 241.
36. Gao, J., et al., *Integrative analysis of complex cancer genomics and clinical profiles using the cBioPortal.* Sci Signal, 2013. **6**(269): p. pl1.
37. Zhu, J., et al., *Gain-of-function p53 mutants co-opt chromatin pathways to drive cancer growth.* Nature, 2015. **525**(7568): p. 206-11.
38. Tomar, S., et al., *ETS1 induction by the microenvironment promotes ovarian cancer metastasis through focal adhesion kinase.* Cancer Lett, 2018. **414**: p. 190-204.
39. Walerych, D., et al., *Proteasome machinery is instrumental in a common gain-of-function program of the p53 missense mutants in cancer.* Nat Cell Biol, 2016. **18**(8): p. 897-909.
40. Palumbo, R., et al., *APEH Inhibition Affects Osteosarcoma Cell Viability via Downregulation of the Proteasome.* Int J Mol Sci, 2016. **17**(10).
41. Singh, K.P., et al., *DNA demethylation by 5-aza-2-deoxycytidine treatment abrogates 17 beta-estradiol-induced cell growth and restores expression of DNA repair genes in human breast cancer cells.* Cancer Lett, 2012. **316**(1): p. 62-9.
42. Ladanyi, A., et al., *Adipocyte-induced CD36 expression drives ovarian cancer progression and metastasis.* Oncogene, 2018. **37**(17): p. 2285-2301.

43. Langmead, B. and S.L. Salzberg, *Fast gapped-read alignment with Bowtie 2.* Nat Methods, 2012. **9**(4): p. 357-9.
44. Consortium, E.P., *An integrated encyclopedia of DNA elements in the human genome.* Nature, 2012. **489**(7414): p. 57-74.
45. Kent, W.J., et al., *The human genome browser at UCSC.* Genome Res, 2002. **12**(6): p. 996-1006.
46. Anders, S., P.T. Pyl, and W. Huber, *HTSeq--a Python framework to work with high-throughput sequencing data.* Bioinformatics, 2015. **31**(2): p. 166-9.
47. Mitra, S., et al., *Transcriptome Profiling Reveals Matrisome Alteration as a Key Feature of Ovarian Cancer Progression.* Cancers (Basel), 2019. **11**(10).
48. Kuhn, E., et al., *TP53 mutations in serous tubal intraepithelial carcinoma and concurrent pelvic high-grade serous carcinoma--evidence supporting the clonal relationship of the two lesions.* J Pathol, 2012. **226**(3): p. 421-6.
49. Domcke, S., et al., *Evaluating cell lines as tumour models by comparison of genomic profiles.* Nat Commun, 2013. **4**: p. 2126.
50. Jin, C., et al., *UCHL1 Is a Putative Tumor Suppressor in Ovarian Cancer Cells and Contributes to Cisplatin Resistance.* J Cancer, 2013. **4**(8): p. 662-70.
51. Obeng, E.A., et al., *Proteasome inhibitors induce a terminal unfolded protein response in multiple myeloma cells.* Blood, 2006. **107**(12): p. 4907-16.
52. Zimmermann, J., et al., *Proteasome inhibitor induced gene expression profiles reveal overexpression of transcriptional regulators ATF3, GADD153 and MAD1.* Oncogene, 2000. **19**(25): p. 2913-2920.
53. Padmanabhan, A., S.A. Vuong, and M. Hochstrasser, *Assembly of an Evolutionarily Conserved Alternative Proteasome Isoform in Human Cells.* Cell Rep, 2016. **14**(12): p. 2962-74.
54. Chui, M.H., et al., *Chromosomal Instability and mTORC1 Activation through PTEN Loss Contribute to Proteotoxic Stress in Ovarian Carcinoma.* Cancer Res, 2019. **79**(21): p. 5536-5549.
55. Su, K.H. and C. Dai, *mTORC1 senses stresses: Coupling stress to proteostasis.* Bioessays, 2017. **39**(5).
56. Poondla, N., et al., *Deubiquitinating enzymes as cancer biomarkers: new therapeutic opportunities?* BMB Rep, 2019. **52**(3): p. 181-189.
57. Sacco, J.J., et al., *Emerging roles of deubiquitinases in cancer-associated pathways.* IUBMB Life, 2010. **62**(2): p. 140-57.
58. Kaushal, K., et al., *Deubiquitinating enzymes in cancer stem cells: functions and targeted inhibition for cancer therapy.* Drug Discov Today, 2018. **23**(12): p. 1974-1982.
59. Reina, C.P., X. Zhong, and R.N. Pittman, *Proteotoxic stress increases nuclear localization of ataxin-3.* Hum Mol Genet, 2010. **19**(2): p. 235-49.
60. Hayashida, N., M. Fujimoto, and A. Nakai, *Transcription factor cooperativity with heat shock factor 1.* Transcription, 2011. **2**(2): p. 91-94.
61. Alam, J. and J.L. Cook, *How many transcription factors does it take to turn on the heme oxygenase-1 gene?* Am J Respir Cell Mol Biol, 2007. **36**(2): p. 166-74.
62. Kawabata, S., et al., *Synergistic effects of nelfinavir and bortezomib on proteotoxic death of NSCLC and multiple myeloma cells.* Cell Death Dis, 2012. **3**: p. e353.
63. Dai, F., et al., *BAP1 inhibits the ER stress gene regulatory network and modulates metabolic stress response.* Proc Natl Acad Sci U S A, 2017. **114**(12): p. 3192-3197.
64. Wei, S., et al., *The activating transcription factor 3 protein suppresses the oncogenic function of mutant p53 proteins.* J Biol Chem, 2014. **289**(13): p. 8947-59.
65. Kawazoe, Y., et al., *Proteasome inhibition leads to the activation of all members of the heat-shock-factor family.* Eur J Biochem, 1998. **255**(2): p. 356-62.

66. Cedar, H. and Y. Bergman, *Linking DNA methylation and histone modification: patterns and paradigms.* Nat Rev Genet, 2009. **10**(5): p. 295-304.
67. Alexandrova, E.M. and N.D. Marchenko, *Mutant p53 - Heat Shock Response Oncogenic Cooperation: A New Mechanism of Cancer Cell Survival.* Front Endocrinol (Lausanne), 2015. **6**: p. 53.
68. Goto, Y., et al., *UCHL1 provides diagnostic and antimetastatic strategies due to its deubiquitinating effect on HIF-1alpha.* Nat Commun, 2015. **6**: p. 6153.
69. Kwan, S.Y., et al., *Ubiquitin Carboxyl-Terminal Hydrolase L1 (UCHL1) Promotes Uterine Serous Cancer Cell Proliferation and Cell Cycle Progression.* Cancers (Basel), 2020. **12**(1).
70. Chou, M.T., et al., *The von Hippel-Lindau Tumor Suppressor Protein Is Destabilized by Src: Implications for Tumor Angiogenesis and Progression.* Genes Cancer, 2010. **1**(3): p. 225-238.
71. Tauriello, D.V. and M.M. Maurice, *The various roles of ubiquitin in Wnt pathway regulation.* Cell Cycle, 2010. **9**(18): p. 3700-9.

Acknowledgements

This work was supported by Liz Tilberis Early Career Award (grant# 544389) from Ovarian Cancer Research Alliance's (SM), Showalter Young Investigator Awards from Ralph W. and Young Grace M. Showalter Trust grant (SM) and Biomedical Research Grant, a pilot grant from Clinical and Translational Science Institute of Indiana University School of Medicine (SM).

The authors are thankful to Dr. Ronny Drapkin, University of Pennsylvania for fallopian tube epithelial cells and STICs. Special thanks to Dr. George Sandusky, Pathology and Laboratory Medicine, IU Health for TMA analysis. We are thankful to Research Immunohistochemistry Facility of IU Health and Ms. Constance J Temm for immunohistochemistry services. We thank Dr. Yunlong Liu, Yue Wang, Xiaona Chu and staff of Center for Medical Genomics for ATAC-sequencing.

Authors' Contribution

Conception and design: Sumegha Mitra
Acquisition of data: Sumegha Mitra, Kinzie Lighty, Apoorva Tangri, Fahmi Mesmar, Marcin Iwanicki
Analysis and Interpretation of data: Sumegha Mitra, Chi Zhang, Fahmi Mesmar, Harikrishna Nakshatri
Manuscript writing and review: Sumegha Mitra, Harikrishna Nakshatri

Figure 1

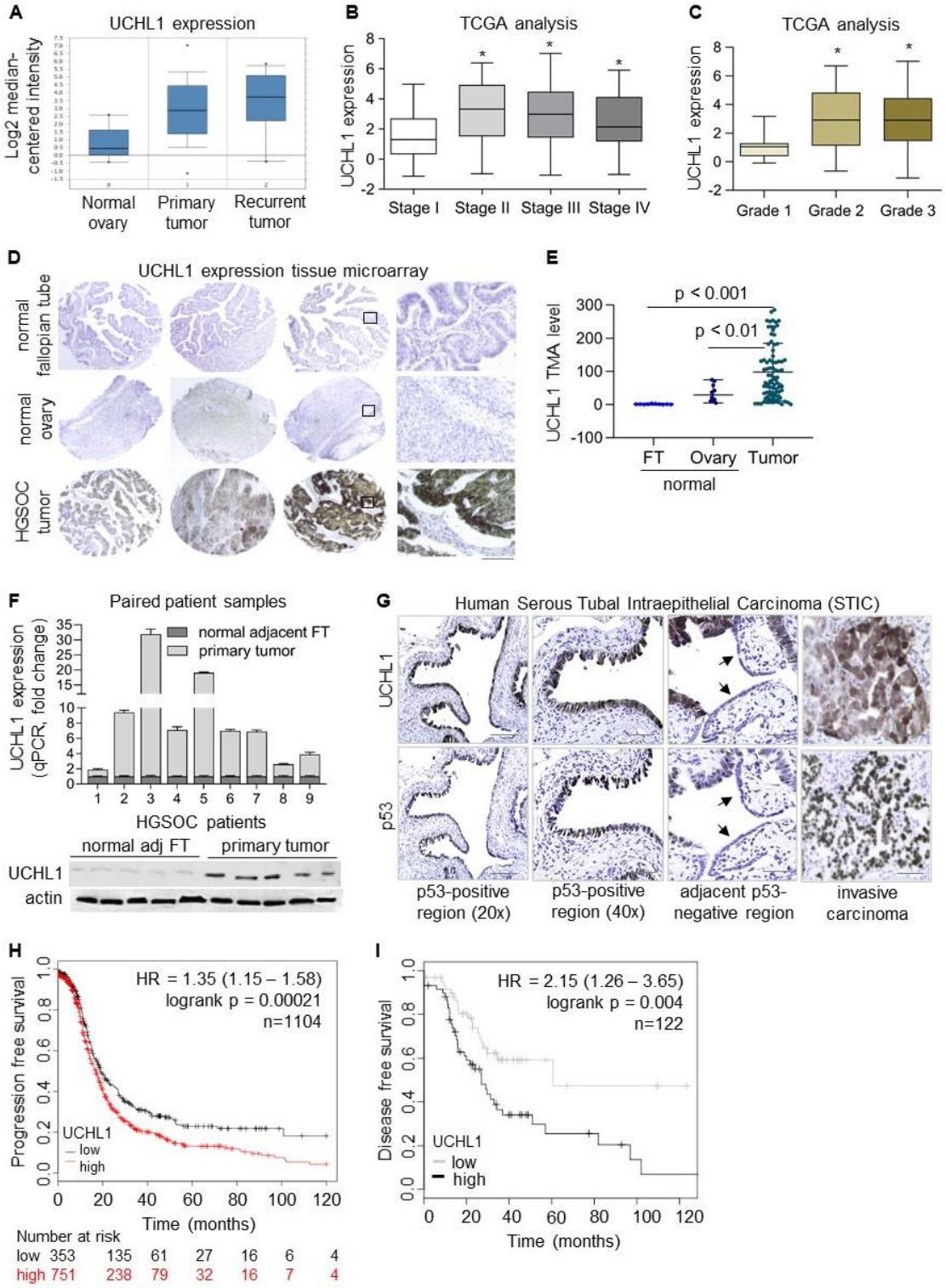

Figure 1. UCHL1 overexpression confers poor prognosis in HGSOC patients. A. UCHL1 mRNA expression in primary and recurrent tumors of HGSOC patients in TCGA database analyzed using the Oncomine gene browser. **B.** UCHL1 expression in stage I (n=16), stage II (n=27), stage III (n=436), and stage IV (n=84) tumors of HGSOC patients in TCGA database. **C.** UCHL1 expression in grade 1 (n=15), grade 2 (n=69) and grade 3 (n=479) tumors of HGSOC patients in TCGA database. **D.** Representative core images for low, medium, and high UCHL1 levels in HGSOC tumors (n=88), normal fallopian tube (FT), and normal ovary (n=10 each) in the tissue microarray (TMA) of HGSOC patients, scale bar: 200µm and 50µm. **E.** Quantification of UCHL1 expression (H-score) by digital scanning of TMA. **F.** Relative UCHL1 mRNA and protein levels in the primary tumor and matched normal adjacent fallopian tube obtained from the same patient (n=9 pairs). Top: qPCR; bottom: western blot (5 pairs) **G.** Representative images of UCHL1 and p53 IHC staining in human serous tubal intraepithelial carcinoma (STIC); scale bar: 50µm and 20µm. **H.** Kaplan Meier survival curves showing progression-free survival of HGSOC patients with low or high UCHL1 levels after optimal and sub-optimal debulking, analyzed by KMplotter ($p = 0.00021$; n=1104). **I.** Survival curves showing disease-free survival of HGSOC patients with low or high UCHL1 levels after optimal debulking, analyzed by OVMARK ($p = 0.004$; n=122). *$p<0.05$. Statistical significance was determined by the Student *t*-test, one-way ANOVA, and the log rank test. The box boundaries represent the upper and lower quartiles, the horizontal line represents the median value, and the whiskers represent the minimum and maximum values.

Figure 2

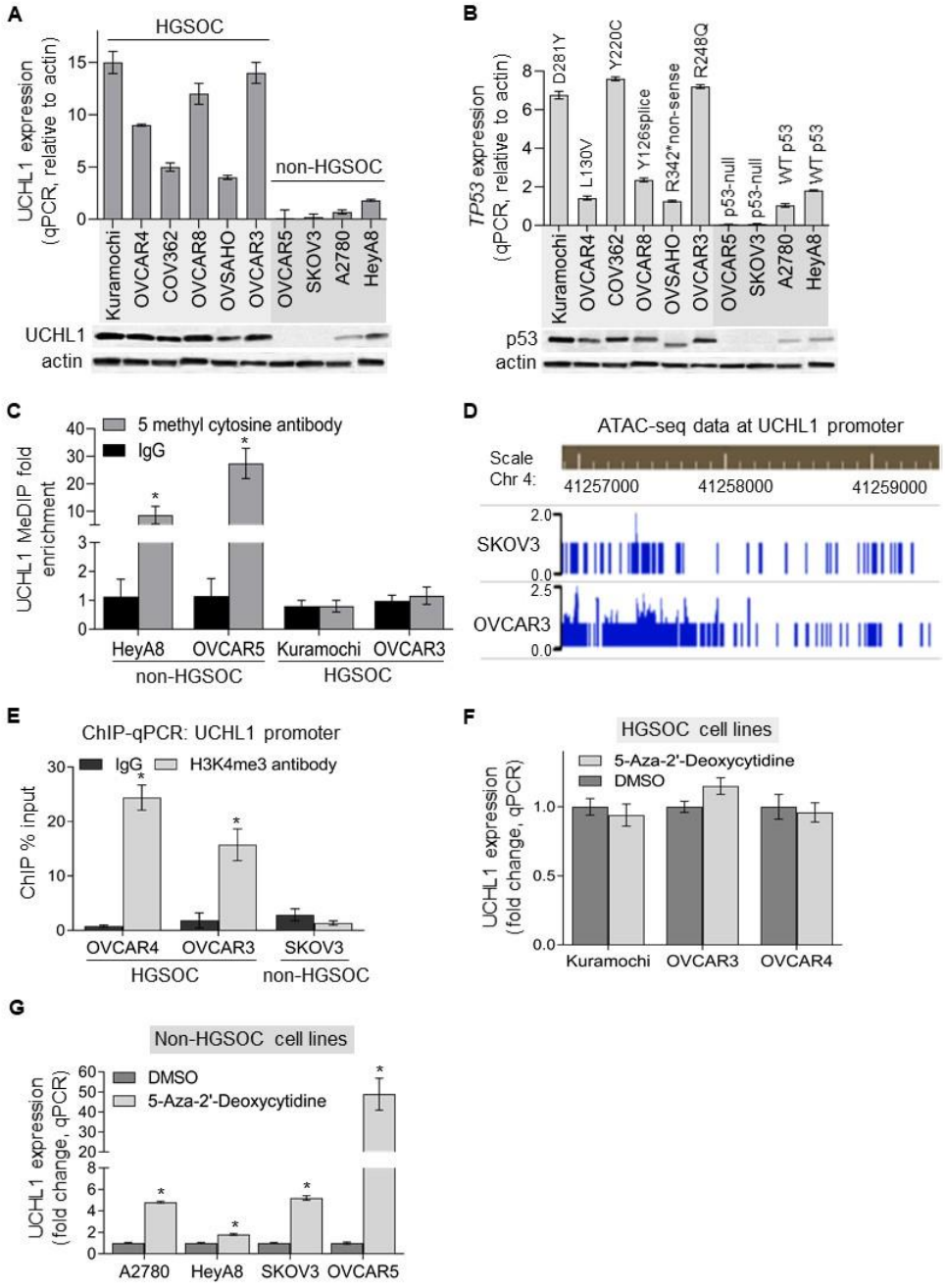

Figure 2. Epigenetic upregulation of UCHL1 in HGSOC. A-B. UCHL1 and p53 mRNA and protein levels in a panel of ovarian cancer cell lines classified as HGSOC and non-HGSOC. Respective p53 mutation in each cell line is given above the bars in (B). **C.** Methylated DNA immunoprecipitation (MeDIP) was performed using 5 methyl cytosine antibody and control IgG in HGSOC and non-HGSOC cell lines followed by MeDIP-qPCR for UCHL1 promoter. Methylated DNA enrichment in the UCHL1 promoter is shown relative to control IgG. **D.** Chromatin accessibility marks on human chromosome 4; region: 41257000-41259000 at UCHL1 gene loci in OVCAR3 and SKOV3 cells identified by ATAC-seq. **E.** Chromatin immunoprecipitation (ChIP) assay was performed using anti-histone H3 trimethyl lysine 4 (H3K4me3) antibody in HGSOC

(OVCAR4 and OVCAR3) and non-HGSOC (SKOV3) cell lines followed by ChIP-qPCR for UCHL1 promoter. H3K4 trimethylated chromatin enrichment in the UCHL1 promoter is shown relative to input. **F-G** UCHL1 expression (qPCR) in DNA methyltransferase inhibitor, 5-Aza-2'-deoxycytidine (5μM, 48h) treated non-HGSOC and HGSOC cell lines. Statistical significance was determined by the Student *t* test from at least three independent experiments. *p<0.05

Figure 3

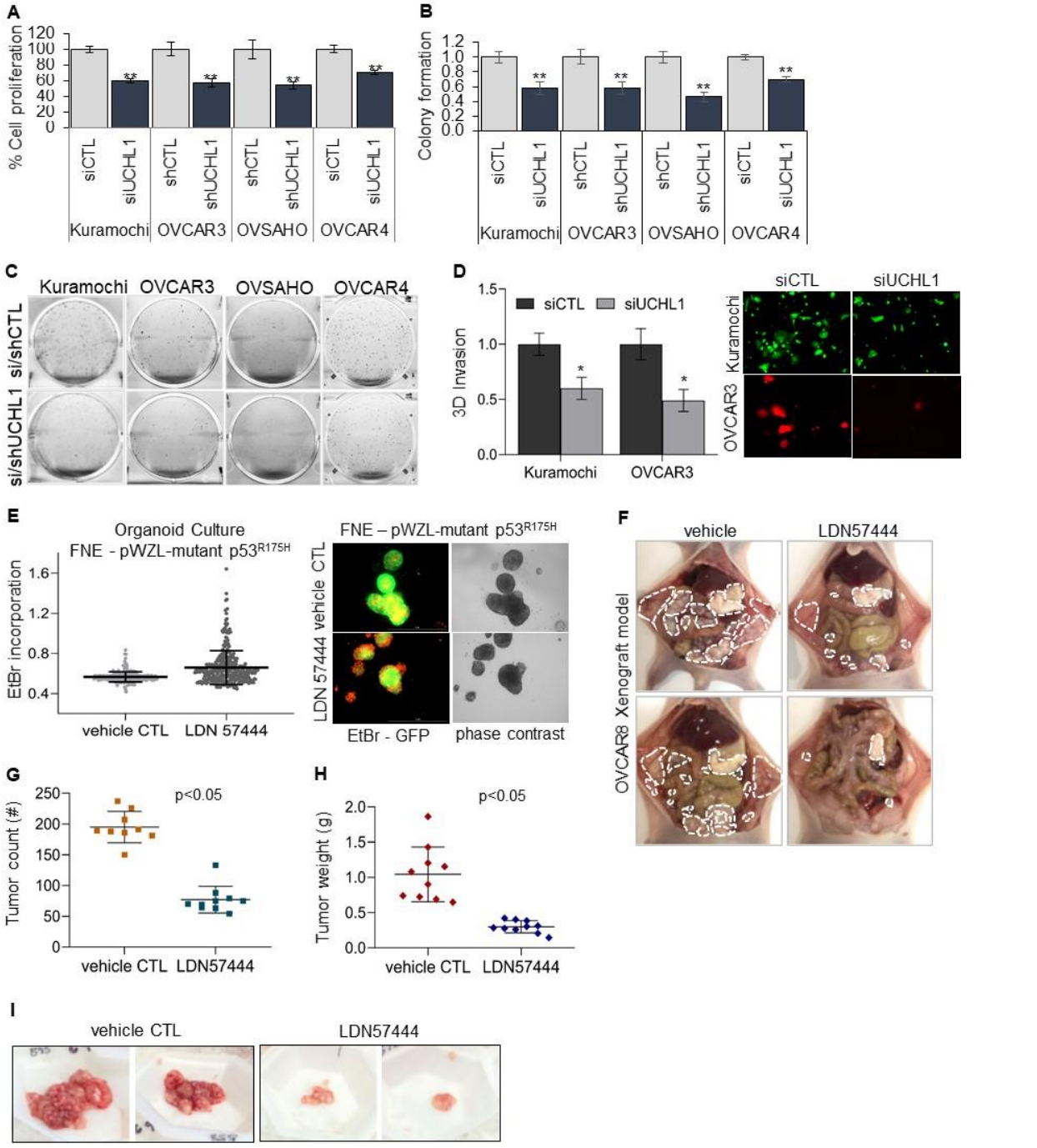

Figure 3. UCHL1 promotes HGSOC growth *in vitro* and *in vivo.* A-B. Relative proliferation and clonogenic growth of HGSOC cells; Kuramochi, OVCAR3, OVCAR4 and OVSAHO transfected or transduced with control or UCHL1 siRNA and control or UCHL1 shRNA lentiviral particles. 2000 cells/well were plated in 96 well plate and MTT assay was performed after 4 days. 1000 cells/well were plated in 6-well plate and colonies were fixed, stained by crystal violet after 8-10 days. **C.** Representative images of colony formation assay of UCHL1 silenced HGSOC cells. **D.** Invasion of OVCAR3 (RFP labelled) and Kuramochi (GFP labelled) cells transfected with control or UCHL1 siRNA through the layers of normal human omental primary mesothelial cells and fibroblasts in a transwell insert (8µm pore size). Invaded cells were fixed after 16h, imaged and counted. **E.** Non-ciliated FT epithelial cells were transfected with pWZL-p53-R175H to overexpress mutant p53 variant R175H. The organoid culture of $FNE^{mutp53\text{-}R175H}$ cells was treated with UCHL1 inhibitor, LDN57444 (LDN, 10µM, 5 days) and vehicle control. Ethidium bromide (EtBr) incorporation was quantified in cellular clusters treated with DMSO (n=254) and LDN (n=334). Representative images of cellular clusters in DMSO and LDN-treated GFP labeled $FNE^{mutp53\text{-}R175H}$ cells. EtBr incorporation is visible as orange color, scale bar 1000 µM. **F.** Representative images of metastatic tumor colonies (encircled in dotted line) in the vehicle control and UCHL1 inhibitor, LDN57444 (LDN; 1mg/Kg) treated mice (n=10 mice/group). **G.** Number of tumor nodules in mice treated with LDN compared to vehicle control. **H.** Weight of surgically resected tumors in vehicle control and LDN-treated mice. **I.** Representative images of surgically resected tumors. **F.** Data shown as mean ± SD. Statistical significance was determined by Student *t* test, *p<0.05, **p<0.001. See Supplementary Figure S3.

Figure 4

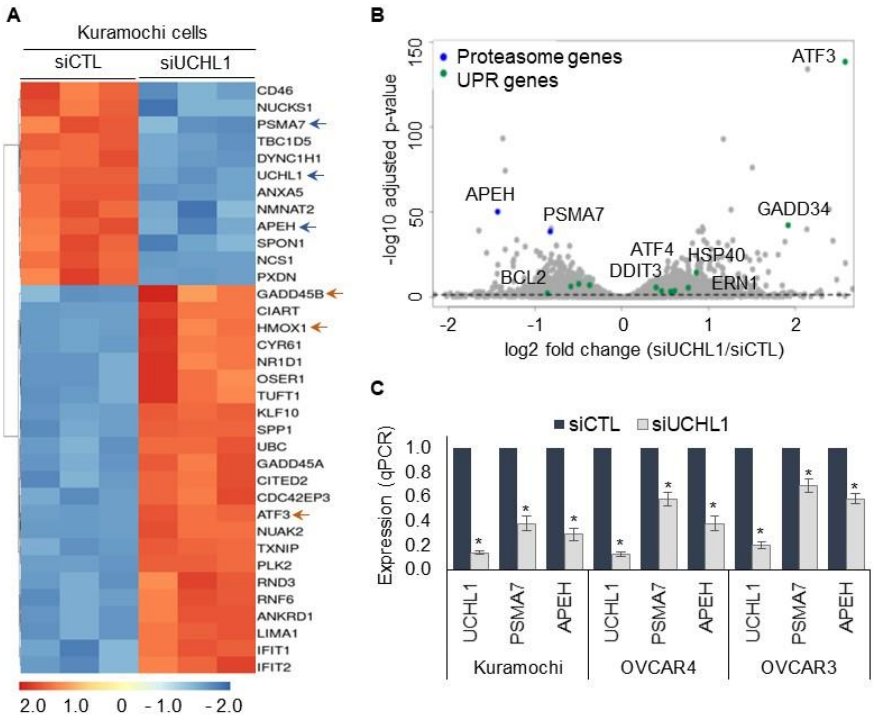

Figure 4. Transcriptional profile of HGSOC cells silenced for UCHL1. A. Heat map representing top 32 differentially expressed genes identified by RNA-sequencing of UCHL1 silenced Kuramochi cells (p<0.005; 1% FDR). Upregulated genes are indicated by orange color, while downregulated genes are indicated by blue color. **B.** Volcano plot representing all the

significantly differentially expressed genes with -log10 (p-values) plotted against log2 fold change values at 1% false discovery rate in UCHL1 silenced Kuramochi cells. For each protein, the x-axis shows the average log2 fold change between siCTL and siUCHL1. The dots on the negative and positive values of x-axis represent downregulated and upregulated genes. Blue dots represent genes implicated with proteasome activity, while the green dots represent ER-stress induced genes. Gray dashed line represents p=0.05 at 1% FDR. Proteins falling above the dashed line are significantly changed.**C.** qPCR validation was performed using taqman assays for PSMA7 and APEH in Kuramochi, OVCAR4, and OVCAR3 cells transfected with CTL or UCHL1 siRNA.

Figure 5

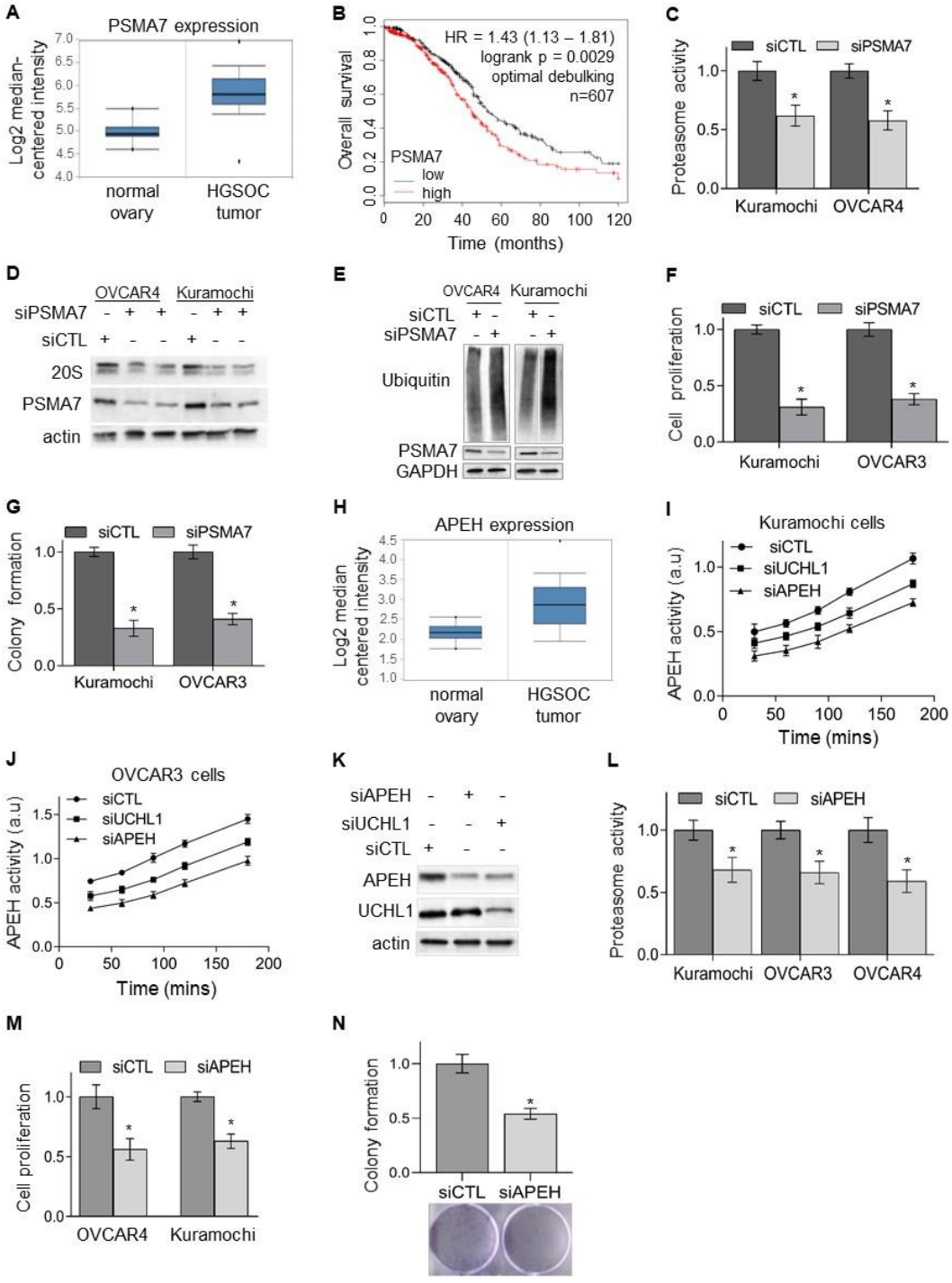

Figure 5. Effect of PSMA7 and APEH on proteasome activity and HGSOC growth. A. PSMA7 mRNA expression in normal ovary and HGSOC patient tumors in TCGA database analyzed using Oncomine gene browser. **B.** Kaplan Meier survival curves showing overall survival of HGSOC patients with low or high PSMA7 levels after optimal debulking analyzed by KMplotter (p = 0.0027, n=607). **C.** Chymotrypsin-like proteasome activity was measured using fluorescent substrate

LLVY-R110 in OVCAR4 and Kuramochi cells transfected with control or PSMA7 siRNA. The cleavage of LLVY-R110 by proteasomes was monitored fluorometrically. **D.** Representative immunoblot analysis of 20S proteasome and PSMA7 in OVCAR4 and Kuramochi HGSOC cells transfected with control or PSMA7 siRNA. **E.** Representative immunoblot analysis of total ubiquitinated proteins in OVCAR4 and Kuramochi HGSOC cells transfected with control or PSMA7 siRNA. **F.** Relative proliferation of HGSOC cells transfected with control or PSMA7 siRNA was measured by MTT assay. **G.** Clonogenic growth of HGSOC cells transfected with control or PSMA7 siRNA. 1000 cells/well were plated in 6-well plate and colonies were fixed, stained by crystal violet after 8-10 days. **H.** APEH mRNA expression in normal ovary and HGSOC patient tumors in TCGA database analyzed using Oncomine gene browser. **I-J.** APEH activity was measured in the total cell lysate of HGSOC cells transfected with control or UCHL1 or APEH siRNA by acetyl-Ala-*p*-nitroanilide (Ac-Ala-pNA). The cleavage of colorimetric p-nitroanilide by APEH was monitored at different time points. **K.** Immunoblot for ubiquitin and analysis of polyubiquitinated proteins in the whole cell lysate of UCHL1 silenced Kuramochi, and OVCAR4 cells. Immunoblot of GAPDH is shown as loading control. **L.** Chymotrypsin-like proteasome activity was measured using fluorescent substrate LLVY-R110 in OVCAR3, OVCAR4 and Kuramochi cells transfected with control or APEH siRNA. The cleavage of LLVY-R110 by proteasomes was monitored fluorometrically. **M.** Relative proliferation of Kuramochi and OVCAR4 cells transfected with control or APEH siRNA was measured by MTT assay. **N.** Colony formation assay was performed for OVCAR4 cells transfected with control or APEH siRNA. 1000 cells/well were plated in 6-well plate and colonies were fixed, stained by crystal violet after 8-10 days. The box boundaries represent the upper and lower quartiles, horizontal line represent the median value, and the whiskers represent the minimum and maximum values. Statistical significance was determined by unpaired Student *t*-test from at least three independent experimental repeats, *p<0.05.

Figure 6

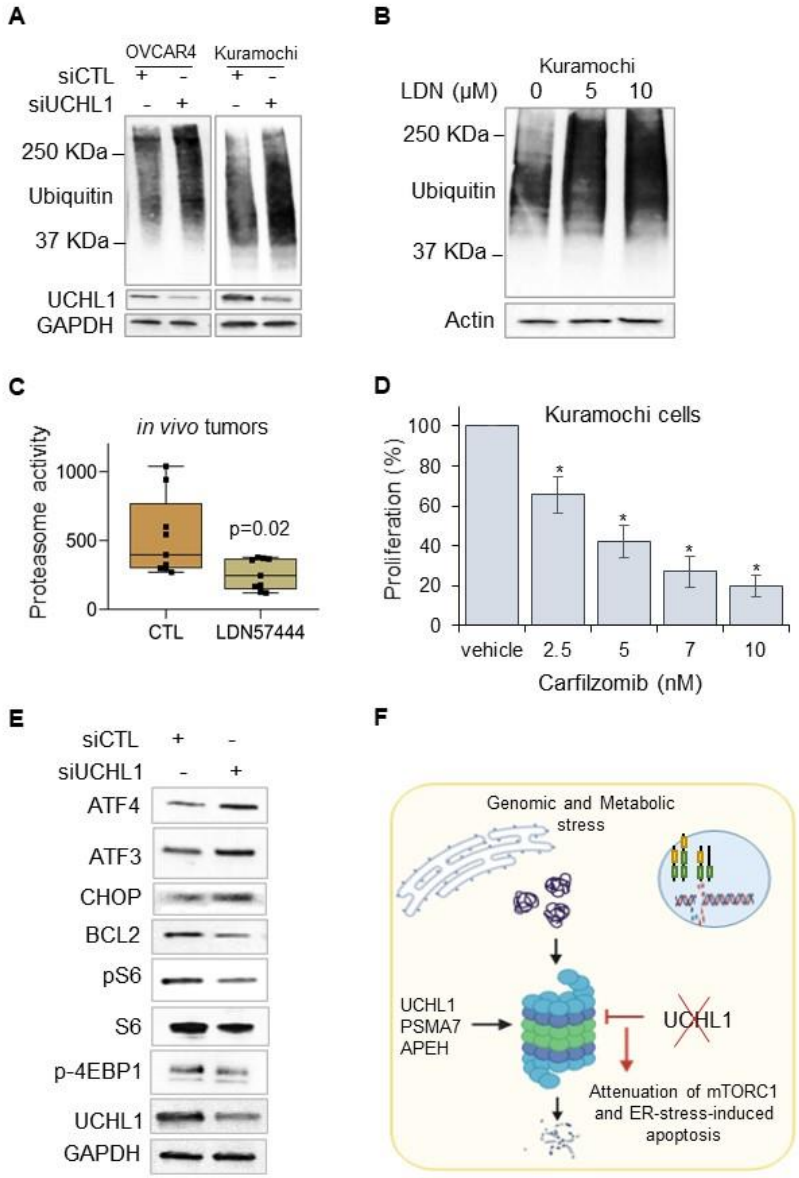

Figure 6. Effect of UCHL1 inhibition on ER stress response and mTORC1 activity. A. Representative immunoblot analysis of total ubiquitinated proteins in OVCAR4 and Kuramochi HGSOC cells transfected with control or UCHL1 siRNA. **B.** Representative immunoblot analysis of total ubiquitinated proteins in Kuramochi cells treated with vehicle control or UCHL1 inhibitor, LDN57444 (5 and 10 μM) for 24 hrs. **C.** Chymotrypsin-like proteasome activity was measured using fluorescent substrate LLVY-R110 in the tissue homogenate of UCHL1 inhibitor, LDN 57444 (LDN) treated xenograft tumors. The cleavage of LLVY-R110 by proteasomes was monitored fluorometrically. **D.** Relative proliferation of Kuramochi cells treated with vehicle control or proteasome inhibitor, carfilzomib was measured by MTT assay after day 3. **E.** Representative immunoblot analysis of target proteins in Kuramochi cells transfected with control or UCHL1 siRNA. **F.** Schematic showing the role of the UCHL1-PSMA7-APEH-proteasome axis in mediating

protein homeostasis. Inhibition of UCHL1 leads to impaired protein degradation and accumulation of proteins resulting in reduced mTORC1 activity, translation and induction of UPR-associated apoptosis.

Supplementary Figure S1

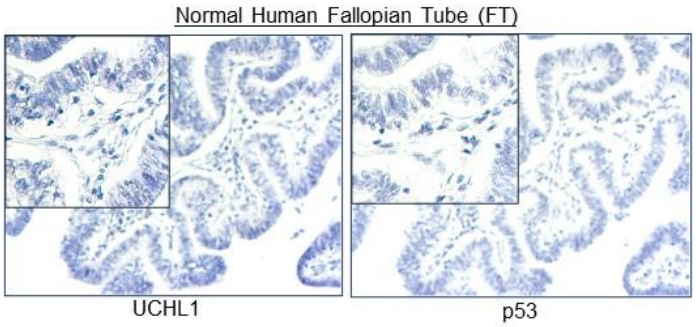

Supplementary Figure S1 (related to Figure 1). Representative image of UCHL1 and p53 immunohistochemical (IHC) staining in the normal human fallopian tube (n=5; 20x; scale bar: 50 µm and 150x magnified inset).

Supplementary Figure S2

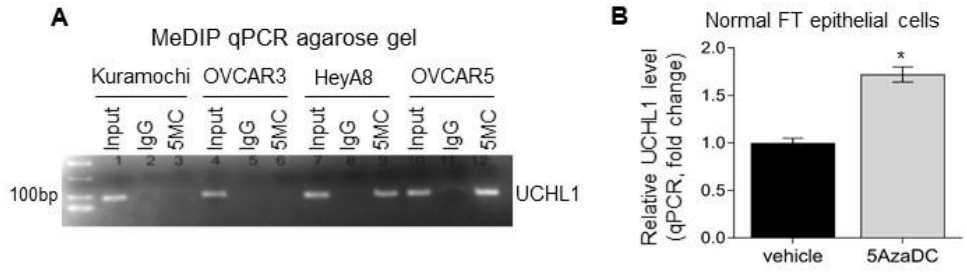

Supplementary Figure S2 (related to Figure 2). A. Medip-qPCR products were resolved in 2% agarose gel with 100bp ladder. Amplification is absent in MeDIP using IgG in all the cell lines, amplification is present in MeDIP using 5MC antibody in non-HGSOC cell lines. **B.** UCHL1 expression (qPCR) in normal human fallopian tube epithelial (FTE) cells treated with 5-Aza-2'-deoxycytidine (5µM, 48h).

Supplementary Figure S3 (related to Figure 3)

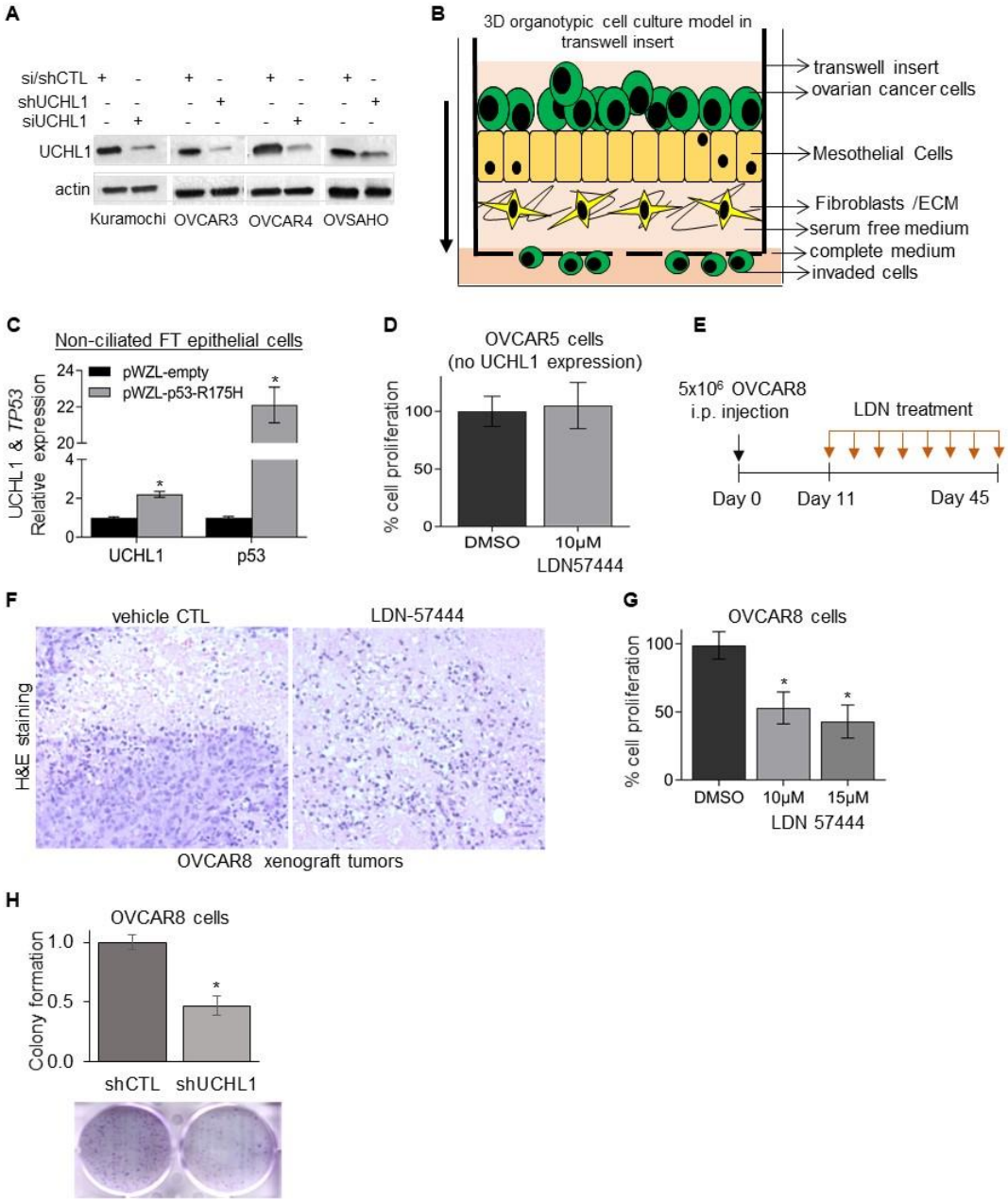

Supplementary Figure S3 (related to Figure 3). A. Immunoblot analysis for UCHL1 in HGSOC cells transfected or transduced with control or UCHL1 siRNA and control or UCHL1 shRNA lentiviral particles. **B.** Schematic of invasion using a 3D organotypic model of human omentum in a transwell insert placed in 24 well plate. HGSOC cells transfected with UCHL1 or control siRNA were plated on the layers of primary human mesothelial cells and fibroblasts embedded in the extra cellular matrix. Cancer cells invaded through omental cells towards complete medium in 24 well plate. **C.** UCHL1 expression (qPCR) in non-ciliated fallopian tube epithelial (FNE) cells

transfected with pWZL-mp53^{R175H} and overexpressing mutant p53 R175H. **D.** Relative proliferation of OVCAR5 (UCHL1 null) cells treated with vehicle control and LDN57444. 2000 cells were plated in 96 well plate and were treated with DMSO and LDN57444 (10µM) on day 1 and day 3, MTT assay was performed on day 4. **E.** Schematic of treatment plan for UCHL1 inhibitor, LDN57444 (LDN) in female athymic nude mice, intraperitoneally injected with $5x10^6$ OVCAR8 cells. **F.** Representative images of hematoxylin and eosin staining in tumors from vehicle control and LDN treated mice. **G.** Relative proliferation of OVCAR8 cells treated with vehicle control and LDN57444. 2000 cells were plated in 96 well plate and were treated with DMSO and LDN57444 (10µM) on day 1 and day 3, MTT assay was performed on day 4. **H.** Relative clonogenic growth of OVCAR8 cells transduced with control or UCHL1 shRNA lentiviral particles. 1000 cells/well were plated in 6-well plate and colonies were fixed, stained by crystal violet after 8 days. Data from at least 3 biological repeats, statistical significance was determined by Student *t* test, *p<0.05.